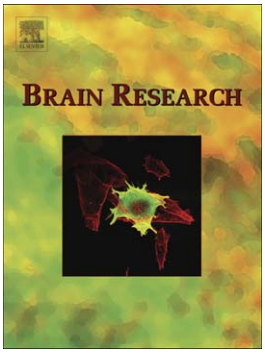

Impaired blood-brain and blood-spinal cord barriers in mutant SOD1-linked ALS rat

Charles Nicaise, Dinko Mitrecic, Pieter Demetter, Robert De Decker, Michèle Authelet, Alain Boom, Roland Pochet

PII: S0006-8993(09)01892-7
DOI: doi:10.1016/j.brainres.2009.09.018
Reference: BRES 39622

To appear in: *Brain Research*

Received date: 3 August 2009
Revised date: 1 September 2009
Accepted date: 4 September 2009

Please cite this article as: Charles Nicaise, Dinko Mitrecic, Pieter Demetter, Robert De Decker, Michèle Authelet, Alain Boom, Roland Pochet, Impaired blood-brain and blood-spinal cord barriers in mutant SOD1-linked ALS rat, *Brain Research* (2009), doi:10.1016/j.brainres.2009.09.018

Impaired blood-brain and blood-spinal cord barriers in mutant SOD1-linked ALS rat

Charles Nicaise[1], Dinko Mitrecic[1], Pieter Demetter[2], Robert De Decker[1], Michèle Authelet[1], Alain Boom[1] and Roland Pochet[1]

[1] *Laboratory of Histology, Neuroanatomy and Neuropathology, Université Libre de Bruxelles, Brussels, Belgium;*

[2] *Department of Pathology, Erasme Hospital, Brussels, Belgium*

E-mail address for each author: cnicaise@ulb.ac.be, dominic@mef.hr, pdemette@ulb.ac.be, rdedecke@ulb.ac.be, mauthele@ulb.ac.be, aboom@ulb.ac.be, rpochet@ulb.ac.be

Corresponding author:

Professor Roland Pochet, PhD

Laboratory of Histology, Neuroanatomy and Neuropathology

808 route de Lennik ; B-1070 Brussels, Belgium

E-mail: rpochet@ulb.ac.be; tel : 32 2 5556374; fax:32 2 5556285.

Abstract

Blood-Brain Barrier (BBB) and Blood-Spinal Cord Barrier (BSCB) impairment is an additional accident occurring during the amyotrophic lateral sclerosis (ALS) progression. In this work we aimed to decipher if BBB/BSCB leakage appeared before critical detrimental events and could serve as a marker preceding clinical symptoms. Three different BBB leakage markers: Evans Blue, IgG and hemosiderin, were used to look at the SOD1-linked ALS rat model at presymptomatic and symptomatic stages. Although IgG and hemosiderin could be detected at presymptomatic stage, Evans Blue extravasation which fits best with BBB/BSCB impairment could only be seen at symptomatic stages. BBB/BSCB impairment was further substantiate by showing at symptomatic stages decreased mRNA expression of ZO-1 and occludin as well as agrin, a basal membrane constituent. Electron microscopic data substantiate a toxic environment around endothelial cell and peri-vascular swollen astrocyte end-feet showing oedema-linked BBB opening.

Classifications terms

Section : Disease-related Neuroscience

Keywords : ALS, mutant SOD1, rat, blood-brain barrier, blood-spinal cord barrier, Evans Blue

Abbreviations

alpha-SMA, alpha-smooth muscle actin; ALS, amyotrophic lateral sclerosis; BBB, blood-brain barrier; BSCB, blood-spinal cord barrier; SOD1, superoxide dismutase 1; ZO-1, zonula occludens-1

1. Introduction

The role of blood vessels in the pathogenesis of amyotrophic lateral sclerosis (ALS) is slowly progressing (for a review see Zlokovic, 2008). The first indication that human blood-brain barrier (BBB) might be affected in ALS came already in 1984 when Leonardi et al. noticed abnormal IgG and albumin levels in patients cerebrospinal fluid (Leonardi et al., 1984). Meanwhile, both IgG and complement protein C3 deposits were discovered in motor cortex and spinal cord from ALS patients (Donnenfeld et al., 1984). In 1990, the presence of IgG in motoneurons and active macrophages was further demonstrated in motor cortex and spinal cord parenchyma which provides evidence of concomitant immune activation in ALS. (Engelhardt and Appel, 1990).

Interestingly, it was also suggested that ALS immunoglobulins might lead to long-lasting troubles at the neuromuscular junction (Uchitel et al., 1992). Furthermore, IgG from ALS patients seemed to induce motor neuron degeneration and Ca2+ enhancement (Engelhardt et al., 1995; Pullen et al., 2004). Blood-derived complement factors seem also to be involved in ALS pathology since C3/C3b and C5a deposits accumulated in $SOD1^{G93A}$ rat spinal cord prior to disease onset (Woodruff et al., 2008).

A step further came recently when Garbuzova-Davis et al. showed Evans Blue leakage around spinal cord microvessels from $SOD1^{G93A}$ mice, clearly indicating dysfunction in endothelia and basement membranes (Garbuzova-Davis et al., 2007a) but the major outcome came from Zhong et al. who showed that disrupted blood-spinal cord barrier came from reduced levels of the tight junction proteins zonula occludens-1 (ZO-1), occludin and claudin-5 between endothelial cells and that endothelial damage accumulated before motor neuron degeneration, suggesting that

it was a central contributor to disease initiation. Evidence of microhemorrhage and hypoperfusion in spinal cord tissue of mutant SOD1 mice was additionally pointed out (Zhong et al., 2008). Toxic blood-borne molecules, e.g. immunoglobulins, complement proteins (Humayun et al., 2009) or thrombin (Festoff et al., 2000), as well as tissue hypoperfusion might be key factors precipitating neuroinflammation, oedema and motoneuronal death observed in ALS. A last report highlighted a similar decreased mRNA expression of tight junction proteins in human ALS spinal cord and strengthened the concept of blood-spinal cord barrier (BSCB) disruption contributing to disease progression (Henkel et al., 2009).

In this work, we have gathered a set of markers of BBB/BSCB integrity (Evans Blue, IgG leakage and hemosiderin deposits), looked at the change of mRNA expression of tight junction and extracellular matrix proteins. We have also explored the ultrastructure of blood vessels from wild-type, presymptomatic (115 days-old) and symptomatic (165 days-old) $SOD1^{G93A}$ rats.

2. Results

2.1. Evans Blue permeability in SOD1^{G93A} brainstem and spinal cord

Blood-brain barrier (BBB) and blood-spinal cord barrier (BSCB) integrity was assessed by perfusing rats with Evans Blue fluorescent dye, which binds to plasma albumin and objectivate vascular leakage. Sensitive Evans Blue quantification showed a significant increase in the brainstem ($p<0.05$) and spinal cord ($p<0.01$) of symptomatic SOD1^{G93A} rats (Figure 1 B) whereas no difference can be detected in age-matched WT and presymptomatic SOD1^{G93A} rats (Figure 1 A). Serial sectioning of brainstem and spinal cord tissue confirmed Evans Blue extravasation around blood vessels in symptomatic SOD1^{G93A} rats (Figure 2 C, F). In WT and presymptomatic rats, very few traces of Evans Blue could be found intravascularly (Figure 2 A-B, D-E). Evans Blue diffusion could barely be depicted around the cerebral ventricles and the choroid plexus but not in the brain parenchyma (data not shown).

2.2. IgG permeability in SOD1^{G93A}brainstem and spinal cord

BBB and BSCB permeability was additionally evaluated using immunohistochemical labeling with anti-rat IgG. As shown in Figure 3, a positive immunoreactivity was found in SOD1^{G93A} brainstem and spinal cord (Figure 3 B-C, E-F). Significant IgG deposits could already be seen at the presymptomatic stage of the disease (Figure 3 B, E). In SOD1^{G93A} rats, IgG immunoreactivity was mainly observed on neuronal cell bodies but also as extracellular IgG aggregates (arrows in Figure 3 E-F). Ventral horns motor neurons were strongly positive for the staining. In SOD1^{G93A} brainstem, immunoreactivity was slightly increased but not depicted in other brain part. Motoneuronal localization of IgG staining was confirmed using SMI-32 antibody

(Tsang et al., 2000). IgG immunoreactivity was found on motoneurons in both brainstem motor nucleus of V and spinal cord of SOD1^{G93A} animals (Figure 3 G, yellow color). Extracellular IgG deposits have also been observed in the ventral horn of SOD1^{G93A} spinal cord (Figure 3 H, white arrow). In contrast, WT animals had very low levels of endogenous IgG in CNS parenchyma (Figure 3 A, D, I). In addition, plasmatic IgG and IgM ($p<0.05$ and $p<0.01$ respectively) levels were slightly increased in SOD1^{G93A} rats (Figure 3 G-H).

2.3. Hemosiderin deposits in SOD1^{G93A} spinal cord

Hemosiderin, a degradation product of haemoglobin, is found in CNS parenchyma under pathological conditions like microhemorrhage. As in SOD1^{G93A} mouse model, blue colored-hemosiderin deposits were found in the rat SOD1^{G93A} spinal cord (Figure 4 B-C). Noteworthy, hemosiderin deposition was variable among animals (see Figure legend); about 50% of SOD1^{G93A} rats did show a positive staining in the spinal cord at presymptomatic or symptomatic stage disease. Deposits were located in the ventral horn around blood vessels and in the vicinity of motor neurons (arrows in Figure 4 B-C). In-depth examination did never highlight the presence of hemosiderin in brainstem or other brain regions.

2.4. mRNA expression of tight junction proteins and agrin in SOD1^{G93A} spinal cord

To further investigate BBB/BSCB disruption, we looked at the gene expression of tight junction proteins occludin and zonula occludens-1 (ZO-1), essential proteins for BBB impermeability. The mRNA expression levels for ZO-1 and occludin were significantly decreased in lumbar spinal cords of symptomatic SOD1^{G93A} rats ($p<0.01$)

but not in presymptomatic SOD1^{G93A} or WT rats (Figure 5 A-B, C-D). No significant change in mRNA expression could be found in brain or brainstem. In order to check the integrity of extracellular matrix, we measured the mRNA expression of agrin, a heparin sulphate proteoglycan localized in the basal lamina of CNS microvessels and involved in the BBB development (Barber et al., 1997). Agrin mRNA was significantly decreased in lumbar spinal cords of symptomatic SOD1^{G93A} rats ($p<0.01$) but not in presymptomatic SOD1^{G93A} or WT rats (Figure 5 D-E).

2.5. Endothelial cells morphology in SOD1^{G93A} rats

Tissue blocks of CNS from WT and SOD1^{G93A} animals were processed for electron microscopic visualization. In WT and presymptomatic SOD1^{G93A} animals, ultrastructure analysis did not reveal significant any blood vessel alterations. All capillaries consisted of a layer of endothelial cells, surrounded by a single layer of basement membrane, and depending of the size of the vessel, vascular smooth cell ensheathment. In symptomatic SOD1^{G93A} rats, severe ultrastructural alterations of endothelial cells were seen throughout the CNS (Figure 6 A). Representative of it is shown in Figure 6 B in which an endothelial cell presented cytoplasmic fragmentation and organelle vacuolization, next to a healthy blood vessel. Mitochondria, as other organelles, in degenerated endothelium, appeared vacuolated and swollen. Abnormal basal membrane replications were also observed, mostly around microvasculature (data not shown). Large blood vessels were surrounded with a continuous sheet of vascular smooth cells whose ultrastructure did not seem altered (see Suppl. Fig. 10). Smooth cell integrity was confirmed using immunohistochemistry of alpha-SMA protein. Under light microscope, alpha-SMA immunoreactivity in the CNS did not suggest any significant alteration between WT,

presymptomatic and symptomatic SOD1^{G93A} rats (see Suppl. Fig. 10). At the electron microscope level, tight junctions appeared intact between morphologically-healthy endothelial cells from WT, presymptomatic or symptomatic SOD1^{G93A} rats (data not shown).

2.6. Swollen astrocyte end-feet in SOD1^{G93A} brain, brainstem and spinal cord

Endothelial abluminal side of *SOD1^{G93A}* blood vessels were regularly surrounded by large white perivascular spaces from presymptomatic stage of disease in all CNS organs (Figure 7 B-C, E-F). At higher magnification, these electron lucent areas appeared to be swollen astrocyte end-feet in close contact with the capillaries (Figure 7 H-I), showing occurrence of oedema and water transport abnormalities. In WT rats, basal membranes of all blood vessels were normally surrounded by well-preserved astrocyte feet without signs of degeneration or swelling (Figure 7 A, D, G).

3. Discussion

In this work we have investigated the BBB/BSCB integrity in the mutant SOD1-linked ALS rat model and its alteration during disease progression. Recent data illustrated that BBB/BSCB impairment is an additional accident occurring during disease progression. As BBB/BSCB functionality and integrity are essential for CNS protection against various harmful blood substances, we aimed to decipher if BBB leakage could serve as a hallmark preceding clinical symptoms. To approach this, we used three different so-called BBB leakage markers: Evans Blue, IgG and hemosiderin, known to substantiate changes in endothelial transport and BBB permeability. Interestingly, differences observed between Evans Blue, IgG and hemosiderin probably reflect slight differences in the transport system used by these molecules to move from blood to brain parenchyma.

IgG extravasation into CNS parenchyma is pathological and usually serves as a marker of BBB/BSCB damage (Baker et al., 2000; Zhang et al., 2001; Zhong et al., 2008), this is why we have used this tool here. However, two other mechanisms of IgG passage should also be considered: one is the reuptake and retrograde axonal transportation by the motoneurons (Fabian and Petroff, 1987; Fratantoni et al., 1996) and the other is transcytosis across endothelial cells (Poduslo et al., 1994). As we did not perform any experiments demonstrating those two alternative pathways, we cannot conclude neither about their happening neither about the ratio (if any) of each to mechanism. Nevertheless, by immunohistochemical labelling, we have found an intense IgG staining both intraneuronally and extracellularly in spinal cord already during the presymptomatic phase of ALS. What causes such extracellular IgG accumulation is presently unknown and deserves further investigations. In addition, IgG accumulation in motoneurons and in extracellular spaces might serve as

microglia activators and trigger the inflammatory cascade hallmarked in ALS (Xu et al., 2009). An ultrastructure study carried on mice inoculated with ALS patient-IgG provided evidence that not only motoneurons seemed to be the target of these endogenous IgG but also endothelial cells in the spinal cord (Engelhardt et al., 2005). Hemosiderin deposits are breakdown products of haemoglobin and reflect previous microhemorrhage occurring under various conditions (Viswanathan and Chabriat, 2006) and therefore might not be specific of the disease. Recent functional studies in ALS-linked mutant SOD1 mice have pointed out a reduced length of capillary and a significant decrease of blood flow in spinal cord which are corroborated with ultrastructural abnormalities showing capillary rupture (Zhong et al., 2008; Garbuzova-Davis et al., 2007b). Similarly to Zhong et al., we have found hemosiderin deposits, in the ventral horn, at close proximity of motoneurons. Hemoglobin seems to be directly toxic to motoneurons via an iron-dependent and oxidative mechanism and its release in CNS parenchyma may contribute to neuronal damage (Regan et al., 1998). Microhemorrhage and hypoperfusion might further lead to chronic hypoxia and even ischemia. It has been shown that these two phenomenons provoke an increased paraendothelial permeability that allows plasma proteins to evasate in the brain tissue (Plateel et al., 1997; Papadopoulos et al., 2001).

Evans Blue forms a conjugate with serum albumin. Albumin transcytosis through brain endothelial cell does not occur. Evans Blue diffusion in the CNS indicates the passage of the dye-protein conjugate through paracellular pathway reflecting increased permeability or damage to BBB. Evans Blue leakage around blood vessels was evident only at symptomatic stage.

The BBB/BSCB impairment was further investigated through variation of expression of tight junction proteins (ZO-1 and occludin), involved in low paracellular

permeability, and agrin, an extracellular protein involved in BBB development (Barber et al., 1997).

According to a recent study, our work confirms a significant loss of expression of occludin and ZO-1 mRNA observed in autopsied human spinal cords from both sporadic and familial forms of ALS (Henkel et al., 2009). This tight junction mRNA downregulation could only be observed in symptomatic $SOD1^{G93A}$ rats although SOD1 mouse model already exhibited decreased protein levels at presymptomatic stage (Zhong et al, 2008). These complementary data validate the results obtained with Evans blue permeability test. The causes of this decrease in structural BBB proteins might be hypothesised when considering the increased levels of chemokines CCL-2/MCP-1 and Il-8 observed in CSF of ALS patients (Kuhle et al., 2009). Zhong et al have suggested that these pro-inflammatory molecules could be mediators of BBB opening. Furthermore, in vitro treatment of bone-marrow microvascular endothelial cells with CCL2/MCP-1 causes a downregulation of tight junction proteins ZO-1 and occludin (Song and Pachter, 2004). Reduced expression of ZO-1 or claudin-5 have been associated with BBB leakage in other neurological disorders such as multiple sclerosis (Kirk et al., 2003) and inflammatory pain (Ronaldson et al., 2009). In middle cerebral artery occlusion animal model, a systemic inflammation caused blood-brain barrier breakdown through disruption of another tight junction protein, claudin-5, but also markedly exacerbated disruption of basement membrane protein (McColl et al., 2008). All these recent data illustrate the concept that ALS-linked inflammatory events contribute to BBB/BSCB opening.

In ALS mouse model, Garbuzova-Davis further showed a loss of basal membrane laminin throughout the spinal cord (Garbuzova-Davis et al., 2007a). This drove us to look at the expression of agrin, a proteoglycan component of basement membrane.

We could confirm that, through agrin decreased expression, a concomitant destructuralization of extracellular matrix occurred. For memory, agrin was originally identified at the neuromuscular junction regulating the clusters of acetylcholine receptors and is significantly downregulated at neuromuscular junction in symptomatic ALS mice (Dobrowolny et al., 2005). Agrin has also been described as being important for the regulation of synaptic processes as well as for the integrity of BBB/BSCB (Barber et al., 1997; Berzin et al., 2000). In case of brain tumor, a partial loss of agrin immunoreactivity occurs concomittaly with BBB breakdown (Rascher et al., 2002).

Finally, comparison between mice and rats SOD1 models indicates that, in both species, IgG and hemosiderin could be seen in spinal cord parenchyma from presymptomatic animals but Evans blue extravasation showed slight discrepancies. Consistently, the same difference appeared when looking at expression of ZO-1 and occludin mRNA. At this stage the difference in species appears the easiest explanation for the difference observed.

In conclusion, in the rat ALS model, at late stage of the disease, a significant increase of Evans blue amount in brainstem and spinal cord could be detected demonstrating a definite BBB/BSCB opening. Due to its late stage appearance, we cannot conclude that this BBB/BSCB opening is causative of the disease but appears rather as a consequence. The hypothesis (to be demonstrated) of the causality of this impairment might be the direct mutant SOD1 toxicity on endothelial cells and/or to other factors (cytokines?) released by the inflammatory process occurring during the last stage of the disease. Our electron microscopic data substantiate a toxic environment around endothelial cell and peri-vascular swollen astrocyte end-feet showing oedema-linked BBB opening (Nicaise et al., 2008)

4. Experimental procedures

4.1. Animals

Wild-type (WT) and transgenic Sprague-Dawley rats (002148-T, NTac:SD-Tg (SOD1G93A) L26H) carrying the mutant human SOD1^{G93A} gene obtained from Taconic Farms were housed in our animal facilities. They were bred and characterized previously in our laboratory (Nicaise et al., 2008). SOD1^{G93A} rats were classified as presymptomatic those without any clinical signs of limb paresis or weight loss at approximately 4 month-old (maximum of weight curve, see Suppl. Fig. 8). Symptomatic SOD1^{G93A} rats showed impaired locomotion with limb paresis and a significant decrease in weight. They had access to food and water ad libidum, were maintained in a 12:12 h day:night cycle and received care in compliance with the national legal requirements and the European Communities Council Directive (86/609/EEC).

4.2. Evans Blue permeability

Evans Blue dye (Merck, Overijse, Belgium) was intravenously injected under light anesthesia using ketamine (40 mg/kg) and xylazine (5 mg/kg). Evans Blue 2% (w/v) in saline (4 ml/kg) was delivered in the caudal vein of the tail through a 24-g catheter, 40 minutes before euthanasia. Euthanasia was achieved under deep anesthesia using ketamine (60 mg/kg) and xylazine (7.5 mg/kg). Rats were intracardially perfused with heparinized saline and thoroughly rinsed during 15 minutes till no more blue dye flew out of the right atrium. Brain, brainstem and spinal cord were removed and divided in two parts for either Evans Blue quantification or visualization.

For sensitive Evans Blue quantification, protocol was adapted from Xu et al. (Xu el al., 2001). Briefly, CNS organs were weighed and kept at -80°C prior to extraction.

Evans blue dye was extracted by incubating brain, brainstem, spinal cord respectively in 2ml, 300µl, 300µl of formamide for 72 hours at 65°C. Extracts were centrifuged at a speed of 13,000 rpm for 10 minutes at 4°C. Supernatant was used for duplicate spectrophotometric measurements at 620 nm and compared to standard curve of Evans Blue in formamide (see Suppl. Fig. 9). Dye concentration was calculated as the ratio of absorbance relative to the amount of tissue.

For Evans Blue visualization, organs were fixed overnight in paraformaldehyde 4% in PBS 0.1M, cryoprotected in sucrose 20%, included in OCT compound and kept at -80°C. Cryostat 20µm-sections were counterstained with DAPI and examined under a Zeiss Axioplan fluorescence microscope.

4.3. Immunohistochemistry and Histochemistry

After fixation of CNS organs in formalin 10% and paraffin-embedding processing, 7µm-sections were rehydrated, endogenous peroxidases were blocked (0.3% H_2O_2 in methanol) and antibody non-specific binding inhibited 2 hours with 10% goat serum.

IgG immunolabelling was performed using a biotinylated goat anti-rat IgG (1:50; Jackson Immunoresearch, Newmarket, UK) for 4 hours, then revealed with avidin-biotin-peroxidase (Vector Labs, Belgium) and diaminobenzidine (DAB; Dako, Belgium), with hematoxylin counterstaining.

Monoclonal anti-alpha-smooth muscle actin (alpha-SMA; 1:100; Novocastra, Zaventem, Belgium) was incubated for 30 minutes and followed by secondary goat anti-polyvalent (Immunologic, Duiven, The Netherlands), staining included avidin-biotin-peroxidase and diaminobenzidine.

Hemosiderin was visualized according to Perls method for iron. Briefly, sections were immersed in potassium ferrocyanide solution 10% (w/v) for 5 minutes, then in a

solution of potassium ferrocyanide 7% (w/v) and hydrochloric acid 3% (v/v) for 20 minutes. After washing in water, sections were counterstained with nuclear fast red for 3 minutes and mounted.

4.4. Immunofluorescence

Organs were freshly removed and fixed overnight in paraformaldehyde 4% in PBS 0.1M, cryoprotected in sucrose 20%, included in OCT compound and kept at -80°C. Cryostat 20µm-sections were immersed in acetone for 5 min, blocked by 10% goat serum for 1 hour at room temperature, and incubated with biotinylated goat anti-rat IgG (1:50; Jackson Immunoresearch, Newmarket, UK) and mouse anti-SMI-32 (1:200; Eurogentec, Seraing, Belgium) for 4 hours. The sections were then washed with PBS and incubated with streptavidine-AlexaFluor 594 (1:100; Molecular Probes, Merelbeke, Belgium) and goat anti-mouse IgG conjugated to fluorescein isothiocyanate (secondary antibody to SMI-32; 1:25; Jackson Immunoresearch). The sections were counterstained with DAPI and examined under a Zeiss Axioplan fluorescence microscope.

4.5. Enzyme-linked immunosorbent assay

Plasma IgG and IgM were measured on heparinized blood samples using a rat IgG or IgM quantitation kit (Bethyl, Montgomery, USA) and following the manufacturer instructions. Briefly, 96-well plates (Maxi-Sorp, NY, USA) were coated with anti-rat IgG or IgM capture antibody (1:100), incubated with diluted plasma samples and antibody binding was detected with an HRP-conjugated secondary antibody (1:50,000) and a TMB colour reaction system. IgG and IgM were measured in duplicate, values extrapolated from supplied standards.

4.6. Quantitative Real-time PCR analysis

Total RNA from brain, brainstem and lumbar spinal cord was extracted using Tripure lysis solution and High Pure RNA Tissue Kit (Roche Diagnostics, Vilvoorde, Belgium) according to the manufacturer's protocol, which included DNase treatment. The mRNA quantification was performed using a two-step real-time reverse-transcriptase polymerase chain reaction on a LightCycler 480. Primers sequences (Table 1) were designed with Primer3 software (Whitehead Institute for Biomedical Research, Cambridge, MA). Quantitative PCR reaction was achieved using commercial kit containing SYBR Green (Eurogentec, Seraing, Belgium) and cycling program was: 5 minutes at 95°C and then 40 cycles, each consisting of 15 seconds at 95°C, and 30 seconds at 60°C. According to the delta delta Ct method, gene expression level of each mRNA was calculated, further normalized to Gapdh and Hprt mRNA, and related to WT control samples. Specific amplification was confirmed by melting curve analysis and migration on agarose gel.

4.7. Ultrastructural analysis in electron microscopy

Euthanasia was achieved under deep anesthesia using ketamine (60 mg/kg) and xylazine (7.5 mg/kg). Rats were intracardially perfused with a solution of paraformaldehyde 2% (w/v) and glutaraldehyde 2% (v/v) in phosphate buffer 0.1M. Brain, brainstem and spinal cord were removed and further fixed in glutaraldehyde 4% (w/v) for 2 hours. After washing in Millonig's buffer containing 0.5% sucrose for 24 hours, tissue blocks were osmicated, dehydrated, embedded in epoxy-resin and cut with a diamond blade on an ultramicrotome. Ultrathin sections collected on nickel

grids were stained with lead citrate and uranium acetate and observed with a Zeiss 109 electron microscope.

4.8. Statistical analyses

Results are expressed as mean ± SEM. Significance ($P<0.05$) was assessed using the Mann-Whitney *U* test. Analysis was achieved with SPSS 11.0 (Chicago, IL).

5. Acknowledgements

This work was granted through FNRS grants n°3.4.545.05 F. Investigators thank Wyeth and ALSA for making ALS animals available.

6. References

1. Baker, E.A., Tian, Y., Adler, S., Verbalis, J. G., 2000. Blood-brain barrier disruption and complement activation in the brain following rapid correction of chronic hyponatremia. Exp. Neurol. 165, 221-230.

2. Barber, A.J. and Lieth, E., 1997. Agrin accumulates in the brain microvascular basal lamina during development of the blood-brain barrier. Dev. Dyn. 208, 62-74.

3. Berzin, T.M., Zipser, B. D., Rafii, M. S., Kuo-Leblanc, V., Yancopoulos, G. D., Glass, D. J., Fallon, J. R., Stopa, E. G., 2000. Agrin and microvascular damage in Alzheimer's disease. Neurobiol. Aging 21, 349-355.

4. Dobrowolny, G., Giacinti, C., Pelosi, L., Nicoletti, C., Winn, N., Barberi, L., Molinaro, M., Rosenthal, N., Musaro, A., 2005. Muscle expression of a local Igf-1 isoform protects motor neurons in an ALS mouse model. J. Cell Biol. 168, 193-199.

5. Donnenfeld, H., Kascsak, R. J., Bartfeld, H., 1984. Deposits of IgG and C3 in the spinal cord and motor cortex of ALS patients. J. Neuroimmunol. 6, 51-57.

6. Engelhardt, J.I. and Appel, S. H., 1990. IgG reactivity in the spinal cord and motor cortex in amyotrophic lateral sclerosis. Arch. Neurol. 47, 1210-1216.

7. Engelhardt, J.I., Siklos, L., Komuves, L., Smith, R. G., Appel, S. H., 1995. Antibodies to calcium channels from ALS patients passively transferred to mice selectively increase intracellular calcium and induce ultrastructural changes in motoneurons. Synapse 20, 185-199.

8. Engelhardt, J.I., Soos, J., Obal, I., Vigh, L., Siklos, L., 2005. Subcellular localization of IgG from the sera of ALS patients in the nervous system. Acta Neurol. Scand. 112, 126-133.

9. Fabian, R. H., Petroff, G., 1987. Intraneuronal IgG in the central nervous system: uptake by retrograde axonal transport. Neurology 37, 1780-1784

10. Festoff, B.W., D'Andrea, M. R., Citron, B. A., Salcedo, R. M., Smirnova, I. V., Andrade-Gordon, P., 2000. Motor neuron cell death in wobbler mutant mice follows overexpression of the G-protein-coupled, protease-activated receptor for thrombin. Mol. Med. 6, 410-429.

11. Fratantoni, S. A., Dubrovsky, A. L., Uchitel, O. D., 1996. Uptake of immunoglobulin G from amyotrophic lateral sclerosis patients by motor nerve terminals in mice. J. Neurol. Sci. 137, 97-102.

12. Garbuzova-Davis, S., Saporta, S., Haller, E., Kolomey, I., Bennett, S. P., Potter, H., Sanberg, P. R., 2007a. Evidence of compromised blood-spinal cord barrier in early and late symptomatic SOD1 mice modeling ALS. PLoS. One. 2, e1205.

13. Garbuzova-Davis, S., Haller, E., Saporta, S., Kolomey, I., Nicosia, S. V., Sanberg, P. R., 2007b. Ultrastructure of blood-brain barrier and blood-spinal cord barrier in SOD1 mice modeling ALS. Brain Res. 1157, 126-137.

14. Henkel, J.S., Beers, D. R., Wen, S., Bowser, R., Appel, S. H., 2009. Decreased mRNA expression of tight junction proteins in lumbar spinal cords of patients with ALS. Neurology 72, 1614-1616.

15. Humayun, S., Gohar, M., Volkening, K., Moisse, K., Leystra-Lantz, C., Mepham, J., McLean, J., Strong, M. J., 2009. The complement factor C5a receptor is upregulated in NFL-/- mouse motor neurons. J. Neuroimmunol. 210, 52-62.

16. Kirk, J., Plumb, J., Mirakhur, M., McQuaid, S., 2003. Tight junctional abnormality in multiple sclerosis white matter affects all calibres of vessel and is associated with blood-brain barrier leakage and active demyelination. J. Pathol. 201, 319-327.

17. Kuhle, J., Lindberg, R. L., Regeniter, A., Mehling, M., Steck, A. J., Kappos, L., Czaplinski, A., 2009. Increased levels of inflammatory chemokines in amyotrophic lateral sclerosis. Eur. J. Neurol. 16, 771-774.

18. Leonardi, A., Abbruzzese, G., Arata, L., Cocito, L., Vische, M., 1984. Cerebrospinal fluid (CSF) findings in amyotrophic lateral sclerosis. J. Neurol. 231, 75-78.

19. McColl, B.W., Rothwell, N. J., Allan, S. M., 2008. Systemic inflammation alters the kinetics of cerebrovascular tight junction disruption after experimental stroke in mice. J. Neurosci. 28, 9451-9462.

20. Nagai, M., Aoki, M., Miyoshi, I., Kato, M., Pasinelli, P., Kasai, N., Brown, R. H., Jr., Itoyama, Y., 2001. Rats expressing human cytosolic copper-zinc superoxide dismutase transgenes with amyotrophic lateral sclerosis: associated mutations develop motor neuron disease. J. Neurosci. 21, 9246-9254.

21. Nicaise, C., Soyfoo, M. S., Authelet, M., De, D. R., Bataveljic, D., Delporte, C., Pochet, R., 2009. Aquaporin-4 overexpression in rat ALS model. Anat. Rec. (Hoboken.) 292, 207-213.

22. Papadopoulos, M.C., Saadoun, S., Davies, D. C., Bell, B. A., 2001. Emerging molecular mechanisms of brain tumour oedema. Br. J. Neurosurg. 15, 101-108.

23. Plateel, M., Teissier, E.,Cecchelli, R., 1997. Hypoxia dramatically increases the nonspecific transport of blood-borne proteins to the brain. J. Neurochem. 68, 874-877.

24. Poduslo, J.F., Curran, G. L., Berg, C. T., 1994. Macromolecular permeability across the blood-nerve and blood-brain barriers. Proc. Natl. Acad. Sci. U. S. A 91, 5705-5709.

25. Pullen, A.H., Demestre, M., Howard, R. S., Orrell, R. W., 2004. Passive transfer of purified IgG from patients with amyotrophic lateral sclerosis to mice results in degeneration of motor neurons accompanied by Ca2+ enhancement. Acta Neuropathol. 107, 35-46.

26. Rascher, G., Fischmann, A., Kroger, S., Duffner, F., Grote, E. H., Wolburg, H., 2002. Extracellular matrix and the blood-brain barrier in glioblastoma multiforme: spatial segregation of tenascin and agrin. Acta Neuropathol. 104, 85-91.

27. Regan, R.F. and Guo, Y., 1998. Toxic effect of hemoglobin on spinal cord neurons in culture. J. Neurotrauma 15, 645-653.

28. Ronaldson, P.T., Demarco, K. M., Sanchez-Covarrubias, L., Solinsky, C. M., Davis, T. P., 2009. Transforming growth factor-beta signaling alters substrate permeability and tight junction protein expression at the blood-brain barrier during inflammatory pain. J. Cereb. Blood Flow Metab 29, 1084-1098.

29. Song, L. and Pachter, J. S., 2004. Monocyte chemoattractant protein-1 alters expression of tight junction-associated proteins in brain microvascular endothelial cells. Microvasc. Res. 67, 78-89.

30. Tsang, Y. M., Chiong, M., Kuznetsov, D., Kasarskis, E., Geula, C., 2000. Motor neurons are rich in non-phosphorylated neurofilaments: cross-species comparison and alterations in ALS. Brain Res. 861, 45-58.

31. Uchitel, O.D., Scornik, F., Protti, D. A., Fumberg, C. G., Alvarez, V., Appel, S. H., 1992. Long-term neuromuscular dysfunction produced by passive transfer of amyotrophic lateral sclerosis immunoglobulins. Neurology 42, 2175-2180.

32. Viswanathan, A. and Chabriat, H., 2006. Cerebral microhemorrhage. Stroke 37, 550-555.

33. Woodruff, T.M., Costantini, K. J., Crane, J. W., Atkin, J. D., Monk, P. N., Taylor, S. M., Noakes, P. G., 2008. The complement factor C5a contributes to pathology in a rat model of amyotrophic lateral sclerosis. J. Immunol. 181, 8727-8734.

34. Xu, L., Guo, Y. S., Liu, Y. L., Wu, S. Y., Yang, C., Wu, D. X., Wu, H. R., Zhang, Y. S., Li, C. Y., 2009. Oxidative stress in immune-mediated motoneuron destruction. Brain Res. [Epub ahead of print]

35. Xu, Q., Qaum, T., Adamis, A. P., 2001. Sensitive blood-retinal barrier breakdown quantitation using Evans blue. Invest Ophthalmol. Vis. Sci. 42, 789-794.

36. Zhang, Y. and Pardridge, W. M., 2001. Mediated efflux of IgG molecules from brain to blood across the blood-brain barrier. J. Neuroimmunol. 114, 168-172.

37. Zhong, Z., Deane, R., Ali, Z., Parisi, M., Shapovalov, Y., O'Banion, M. K., Stojanovic, K., Sagare, A., Boillee, S., Cleveland, D. W., Zlokovic, B. V., 2008. ALS-causing SOD1 mutants generate vascular changes prior to motor neuron degeneration. Nat. Neurosci. 11, 420-422.

38. Zlokovic, B.V., 2008. The blood-brain barrier in health and chronic neurodegenerative disorders. Neuron 57, 178-201.

Figure legends

Fig. 1. Evans Blue permeability quantification in three different CNS regions from presymptomatic (A), symptomatic SOD1^{G93A} rats (B) and age-matched WT rats. Forty minutes after Evans Blue intravenous injection, WT rats (*n*=5), presymptomatic (*n*=4) and symptomatic (*n*=4) SOD1^{G93A} rats were sacrificed and thoroughly rinsed with saline. Evans Blue quantity was calculated using a standard curve (see Suppl. Fig. 8). A significant increase was seen in brainstem and spinal cord but not in the brain of symptomatic SOD1^{G93A} rats. Results are expressed as means±SEM of Evans Blue quantity relative to amount of tissue weight. $^{**}P<0.01$; $^{*}P<0.05$.

Fig. 2. Evans Blue leakage in the brainstem (A, B, C) and in the lumbar spinal cord (D, E, F) of WT rats (A, D), presymptomatic (B, E) and symptomatic SOD1^{G93A} rats (C, F). The nuclei were counterstained with DAPI and dashed lines indicated blood vessels. Evans Blue red fluorescence was detected in extravascular spaces of brainstem and spinal cord from symptomatic SOD1^{G93A} rats. WT and presymptomatic SOD1^{G93A} rats barely showed intravascular Evans Blue dye. Illustrations are representative of 5 independent rats in each group (scale bar = 25µm).

Fig. 3. IgG immunoreactivity in the brainstem (A, B, C) and in the lumbar spinal cord (D, E, F) of WT rats (A, D), presymptomatic (B, E) and symptomatic SOD1^{G93A} rats (C, F). Both presymptomatic and symptomatic SOD1^{G93A} rats exhibited IgG deposits in brainstem and spinal cord regions compared to WT rats devoided of immunoreactivity. Motoneurons from motor nucleus of V (B, C) were positive in the brainstem of SOD1^{G93A} rats. Intraneuronal and extracellular IgG deposits (black arrows; E, F) could be observed in the spinal cord of all SOD1^{G93A} rats. IgG (red) and

SMI-32 (motoneuron marker, green) double immunostaining in SOD1^{G93A} rats. Merged (yellow) indicates motoneuronal-associated IgG staining. Motoneurons from motor nucleus of V were double positive in the brainstem of SOD1^{G93A} rats (G). Intraneuronal (yellow) and extracellular (white arrow) IgG deposits could be observed in SOD1^{G93A} spinal cords (H). In contrast, WT animals did not show any IgG staining (I). Illustrations are representative of at least 5 independent rats in each group. Scale bar represents 100μm in A, B, C, G and 50μm in D, E, F, H, I. Symptomatic SOD1^{G93A} rats showed significant increased concentrations of plasma IgG (J) and IgM (K). Concentrations were measured by quantitative sandwich ELISA and expressed as means±SEM in g/L. $^{**}P<0.01$; $^{*}P<0.05$.

Fig. 4. Hemosiderin deposition in the lumbar spinal cord of SOD1^{G93A} rats. Extracellular blue deposits (arrows) of haemoglobin derivatives have been sparsely found in the ventral horn of spinal cord from SOD1^{G93A} rats at both presymptomatic (B) and symptomatic (C) stages but not in WT rats (A) (scale bar = 50μm). Blue dots, reflecting hemosiderin deposits in the tissue, were found in 0 on 10 WT animals (0%), in 3 on 5 presymptomatic (60%) and in 7 on 15 symptomatic (46.66%) SOD1^{G93A} rats.

Fig 5. mRNA expression of occludin, zonula occludens-1 (ZO-1) and agrin in brain, brainstem and spinal cord from WT (n=4), presymptomatic (n=4) and symptomatic (n=8) SOD1^{G93A} rats. mRNA expression levels for ZO-1, occludin and agrin were decreased in lumbar spinal cords of symptomatic SOD1^{G93A} rats but not in presymptomatic SOD1^{G93A} or WT rats. No significant change in mRNA expression was found in brain or brainstem. mRNA copies were normalized to Gapdh and fold-

change expressed relative to control WT rats. Equivalent results and significance were obtained using Hprt as housekeeping gene. Bars represent means±SEM. $^{**}P<0.01$.

Fig. 6. Electron micrographs showing endothelial cells in spinal cord of symptomatic $SOD1^{G93A}$ rats (A, B). Many endothelial cells belonging to small blood vessels (bv) underwent cell death with cytoplasmic fragmentation and packing of their organelles. In panel A, degenerated endothelial cell with cytoplasmic fragmentation in the left capillary (cy1) while endothelial cell with healthy cytoplasm (cy2) can also be observed on the right blood vessel. In panel B, altered endothelial cell on the right (cy3) is next to a healthy endothelial cell on the left capillary (cy4). No abnormalities were found in presymptomatic $SOD1^{G93A}$ rats or in WT rats. Illustrations are representative of 2 independent rats in each group (scale bar = 2µm). Bv, blood vessel; cy, cytoplasm; N, nucleus.

Fig. 7. Electron micrographs showing capillaries from cerebral cortex (A, B, C), brainstem (D, E, F) and spinal cord (G, H, I) of presymptomatic (B, E, H), symptomatic (C, F, I) $SOD1^{G93A}$ rats compared to WT rats (A, D, G). In $SOD1^{G93A}$ rats, swollen astrocyte end-feet (asterisks in B, C, E, F, H, I) could be observed within CNS parenchyma as soon as presymptomatic stage. Illustrations are representative of 2 independent rats in each group (scale bar = 2µm).

Supplementary figures

Fig. 8. Relative mean body weight of SOD1^{G93A} rats. Relative weight means the ratio between the actual weight and the maximum weight in life. Animals are considered as presymptomatic before weight decline at about 4 month-old. Symptomatic stage of SOD1^{G93A} rats is characterized by locomotor deficit and limb paralysis and can last up to 6 month-old. Symbols represent mean ± SEM from *n*=8 animals.

Fig. 9. Evans Blue standard curve in formamide as a function of concentration from 7.8 to 1000 ng/ml. Absorbance of Evans Blue dye was measured at 620 nm.

Fig 10. Immunolabelling of vascular smooth cells using alpha-smooth muscle actin antibody (alpha-SMA) in the lumbar spinal cord of WT (A) and SOD1^{G93A} rats (B). Smooth cells around large blood vessels were labelled similarly (arrowheads) in the ventral horn spinal cord of presymptomatic, symptomatic SOD1^{G93A} rats compared to WT rats (scale bar = 50µm). Illustrations are representative of 5 independent rats in each group. Electron micrograph from symptomatic SOD1^{G93A} spinal cord showing intact vascular smooth cell (Vsc) morphology between a swollen astrocyte end-foot (asterisk) and an endothelial cell (C).

Table 1.

Gene Accession N°	**Sense**	**Antisense**
Agrin NM_175754	5'-AGTCAGTGGGGGACTCAGAAA-3'	5'-GCAGTGCCTTCTCACTCTCAA-3'
Gapdh NM_017008	5'-AATGTATCCGTTGTGGATCT-3'	5'-CAAGAAGGTGGTGAAGCAGG-3'
Hprt NM_012583	5'-GGACCTCTCGAAGTGTTGGAT-3'	5'-CCAACAACAAACTTGTCTGGAA-3'
Occludin NM_031329	5'-TGATTCGGATCCTGTCTATGC-3'	5'-ATAGGCTCTGTCCCAAGCAAG-3'
ZO-1 NM_001106266	5'-CCTCTGATCATTCCACACAGTC-3'	5'-TAGACATGCGCTCTTCCTCTCT-3'

Table 1. Primer sequences. Abbreviations : Gapdh, glyceraldehyde 3-phosphate dehydrogenase ; Hprt, hypoxanthine-guanine phosphoribosyltransferase ; ZO-1, zonula occludens-1.

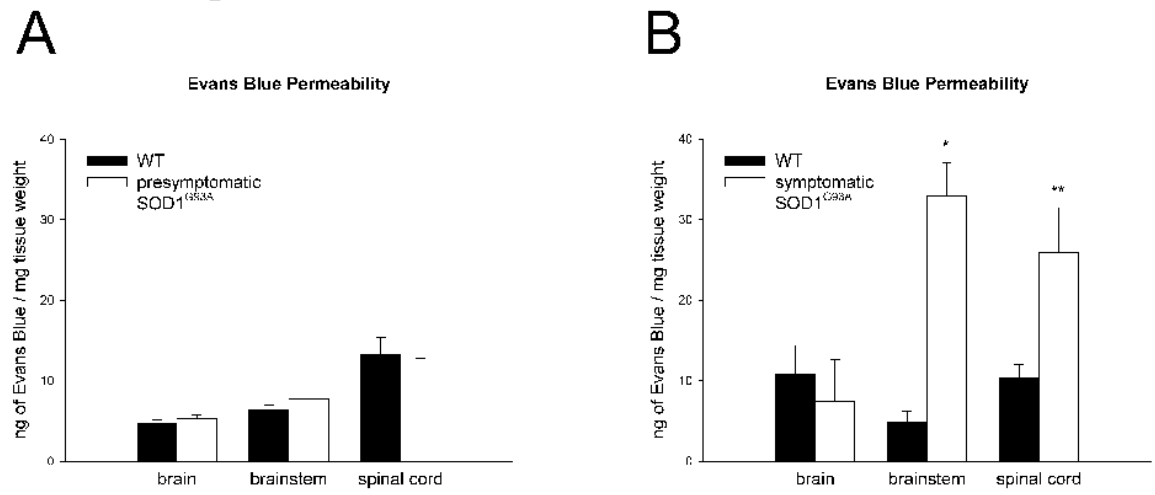

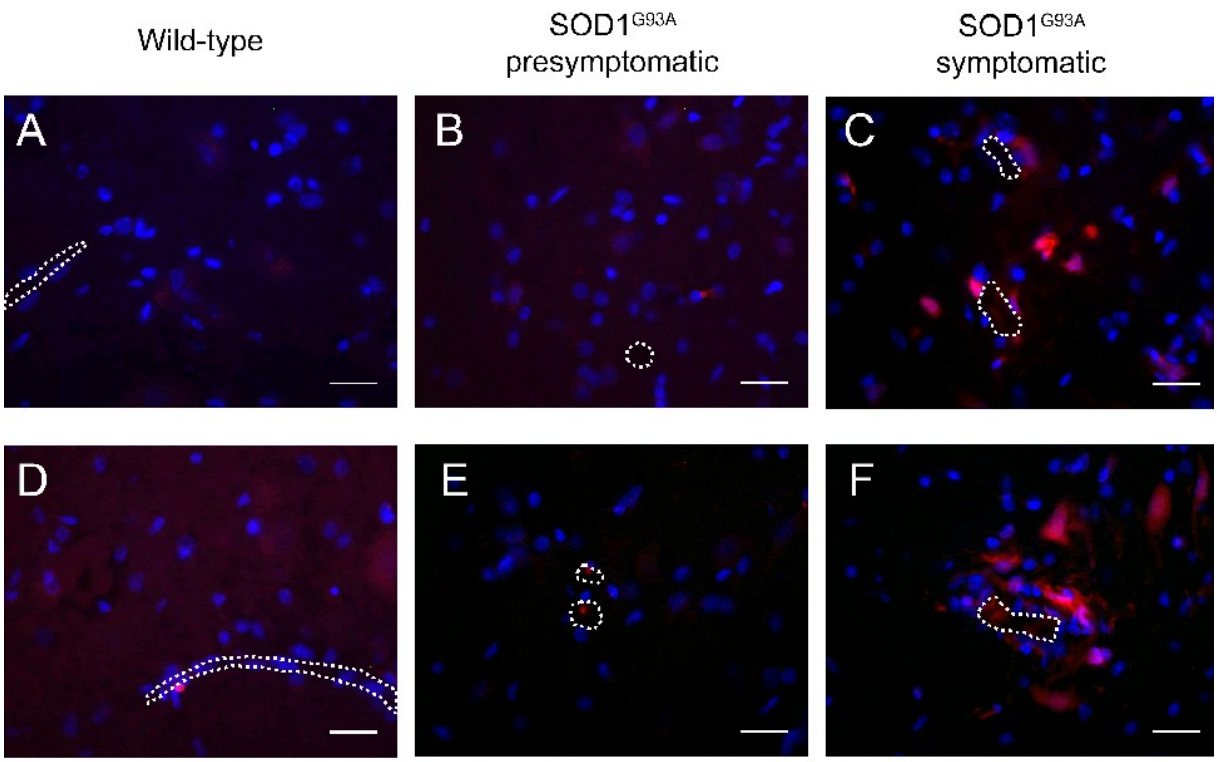

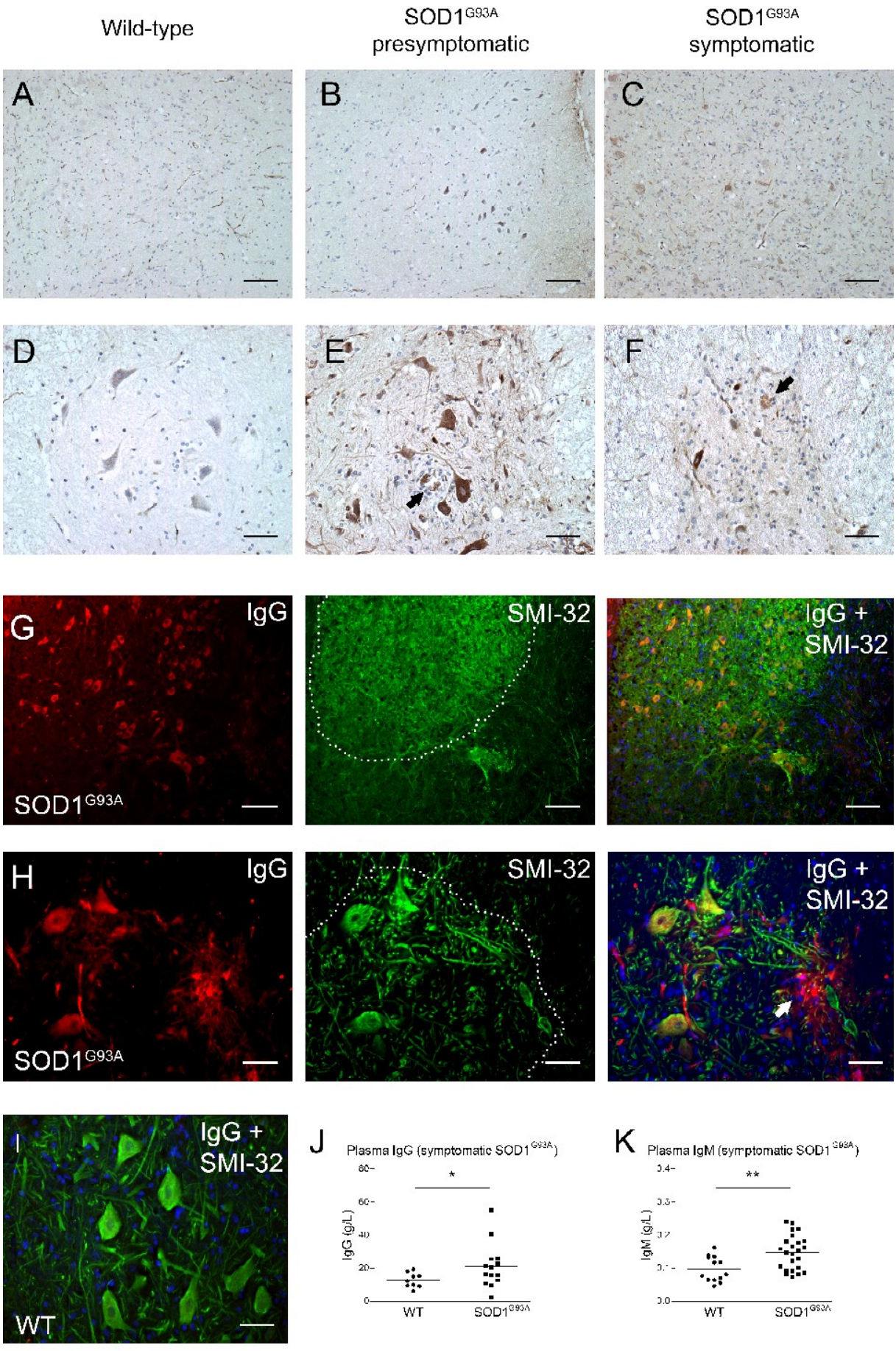

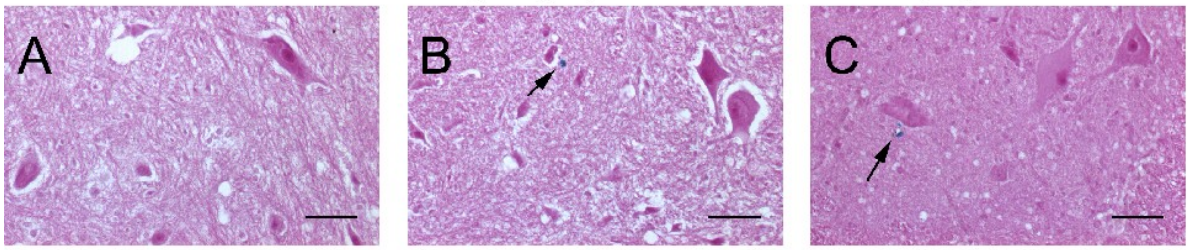

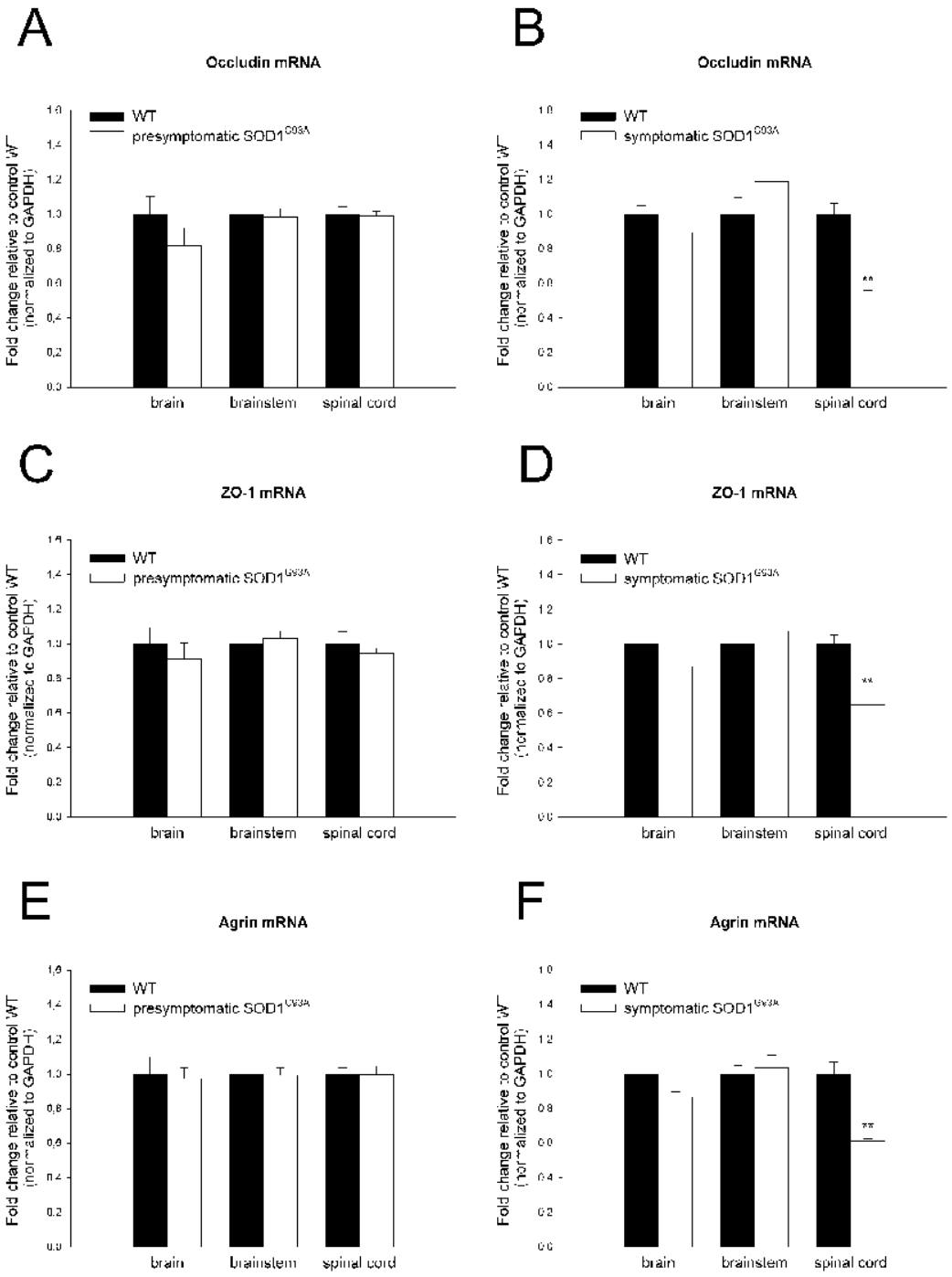

SOD1^{G93A} symptomatic